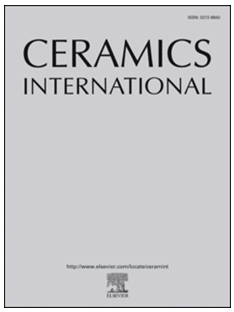

Energy harvesting using lead-free multilayer piezo stacks based on $0.95(Bi_{0.5}Na_{0.5})TiO_3$-$0.05(BaTiO_3)$ piezoceramics through the addition of ZrO_2

Santiago Osinaga, Mauro Difeo, Mariano Febbo, Miriam Castro, Leandro Ramajo, Sebastián Machado

PII: S0272-8842(24)00941-6

DOI: https://doi.org/10.1016/j.ceramint.2024.03.025

Reference: CERI 40186

To appear in: *Ceramics International*

Received Date: 26 December 2023

Revised Date: 28 February 2024

Accepted Date: 3 March 2024

Please cite this article as: S. Osinaga, M. Difeo, M. Febbo, M. Castro, L. Ramajo, Sebastiá. Machado, Energy harvesting using lead-free multilayer piezo stacks based on $0.95(Bi_{0.5}Na_{0.5})TiO_3$-$0.05(BaTiO_3)$ piezoceramics through the addition of ZrO_2, *Ceramics International* (2024), doi: https://doi.org/10.1016/j.ceramint.2024.03.025.

Energy harvesting using lead-free multilayer piezo stacks based on $0.95(Bi_{0.5}Na_{0.5})TiO_3$-$0.05(BaTiO_3)$ piezoceramics through the addition of ZrO_2

Santiago Osinaga[a*], Mauro Difeo[b*], Mariano Febbo[c], Miriam Castro[b], Leandro Ramajo[b], Sebastián Machado[a]

[a]*Grupo de Investigación en Multifísica Aplicada, Universidad Tecnológica Nacional, Facultad Regional Bahía Blanca, CIC. 11 de Abril 461, Bahía Blanca, Argentina*

[b]*Instituto de Investigaciones en Ciencia y Tecnología de Materiales (INTEMA), Av. Colón 10850, Mar del Plata, B7606BWV, Argentina*

[c]*Instituto de Física del Sur (IFISUR), Universidad Nacional del Sur (UNS), Bahía Blanca, B8000CPB, Argentina.*

***Corresponding authors.**

E-mail: smosinaga@frbb.utn.edu.ar, maurodifeo@fi.mdp.edu.ar

Abstract:

This paper explores the feasibility of utilizing lead-free multilayer piezo stacks, particularly focusing on Zr-doped $0.95(Bi_{0.5}Na_{0.5})TiO_3$-$0.05(BaTiO_3)$ piezoceramics, for energy harvesting. Various lead-free BNT-BT disk samples with different Zr concentrations undergo structural, microstructural, and electrical characterizations. The results illustrate that Zr-doping improves piezoelectric constitutive parameters, notably at a 2.0 mol% concentration. Electromechanical tests were conducted on multilayer piezo stacks, involving variations in electric load, mechanical load, frequency, and number of stacked disks. These tests demonstrate the ability of the multilayer transducer to produce up to 1.5 Volts (peak) under particular conditions: a 250 Hz frequency, a 10 N mechanical load, and an open circuit electric load, utilizing a stack comprising 5 disks. Employing an

analytical mathematical model, an effective d_{33}^{eff} of the system is determined, yielding values ranging from 588 to 625 pC/N for a stack composed of 5 disks. These findings highlight the considerable potential of lead-free multilayer piezo stacks in energy harvesting applications, offering crucial insights for the development of sustainable and eco-friendly energy solutions.

Keywords: lead–free piezoceramic, energy harvesting, multilayer piezo stack transducer, zirconium doping.

1 Introduction

The increasing demand for sustainable and renewable energy sources has led to a surge in research and development of technologies aimed at scavenging ambient energy. Among the diverse mechanisms for Energy Harvesting (EH), piezoelectric materials stand out for their unique ability to directly convert mechanical vibrations into electrical energy, presenting an efficient and environmentally friendly alternative [1].

In the past decade, the potential for harvesting energy using different piezoelectric devices has been explored. Examples include the cantilever beam [2], cymbal [3], bridge [4], or commercial options like interdigitated electrodes (Macro Fiber Composite [5]), QuickPADs (MIDÉ Technology [6]), or piezocomposites (APC International [7]). Recently, multilayer or piezo stack transducers have gained attention for energy harvesting applications [8]. Structurally, they consist of an arrangement of piezoceramic disks or squares and electrode layers, both with very small thicknesses, interleaved consecutively.

Among the main advantages associated with multilayer actuators, their high actuation speed and high-resolution positioning stand out; making them particularly useful for applications such as nano-positioning and microscopy. On the other hand, as a generator, their benefits could be associated with their great capacity to withstand forces (compared with bulk ceramics) and high capacitance. Currently, several commercial brands manufacture multilayer actuators with more than 100 layers, each with a thickness of the order of nanometers [9, 10]. Alternatively, some researchers have constructed their transducers from bulk piezoceramics and interleaved electrodes, with a significantly lower number of layers reaching improved energy generation levels [11, 12].

The selected piezoelectric material significantly influences the performance of energy harvesting devices. Commonly, PZT-based (Lead zirconate titanate) materials are used due to their chemical stability, excellent piezoelectric properties, and reasonable cost [13]. Nevertheless, the presence of

lead oxide in PZT poses a significant health risk, as its toxicity is intensified when it vaporizes at elevated temperatures, especially during the processes of calcination and sintering, leading to environmental pollution [14]. In this direction, lead-free alternatives have captured the attention due to their environmental benefits: the elimination of lead mitigates concerns regarding toxicity and environmental impact, aligning with the growing emphasis on green technologies.

Among lead-free materials, $Bi_{0.5}Na_{0.5}TiO_3$ (BNT)-based ceramics have been widely studied for piezoelectric applications [15]. At room temperature, BNT has a perovskite structure with a ferroelectric rhombohedral symmetry, a relatively high coercive electric field of ~73 kV/cm, large remnant polarization (Pr = 38 μC/cm^2), and a Curie temperature of ~320 °C [16]. However, the large coercive field and high conductivity hinder the polarization for industrial applications. On the other hand, $BaTiO_3$ (BT) has a perovskite structure with a ferroelectric tetragonal symmetry at room temperature and a Curie temperature close to 130 °C [17]. Consequently, to enhance the piezoelectric properties of BNT ceramics, $(1-x)(Bi_{0.5}Na_{0.5})TiO_3$-$x(BaTiO_3)$ (BNT-BT) solid solution stands out as a promising candidate to replace PZT-based materials [18], due to the possible stabilization of a morphotropic phase boundary (MPB) where coexist the rhombohedral and tetragonal phases [17]. Simultaneously, the scientific community is currently investigating the benefits of different additives to improve the electrical properties of the BNT-BT solid solution [19,20]. Especially under the appropriate doping levels, there exists a potential to enhance the piezoelectric properties by changes in the densification, the microstructure, and/or crystal chemistry defects. For example, the addition of lithium [21] or CuO [22] decreases the sintering temperature of BNT-BT ceramics, whereas Al_2O_3 or MnO_2 promotes the grain growth and improves the electrical properties of the ceramics [19,20], and B_2O_3 addition improves the densification and the piezoelectric properties by modifying the defect chemistry [20]. Zr-doping significantly influences the dielectric properties and structural characteristics in BaTiO3-based ceramics observing a corresponding decrease in spontaneous polarization and twinned domain structures in fine-grained ceramics. These samples also showed a

flattened permittivity response with temperature and significantly lower losses [23]. Furthermore, Rachakom et. al [24] determined that a small addition of Zr into BNT-based ceramics raised the dielectric constant value. A high Zr concentration induced more unit cell distortion which caused the degradation of dielectric properties. Poling also had some effects on the ferroelectric behavior of Zr-doped BNT (BNTZ) ceramics, particularly in the rhombohedral phase region in terms of improved breakdown strength. Yao et al. [25] investigated the structural and piezoelectric properties of $(Bi_{0.5}Na_{0.5})_{0.94}Ba_{0.06}Zr_yTi_{1-y}O_3$ piezoceramics, where a relaxor-like behavior was observed. Effectively, a diminution in the remnant polarization and coercive field values, and the additional disappearance of piezoelectric properties were found by the substitution of 2 and 4 mol % Zr^{4+} for Ti^{4+}.

The integration of lead-free ceramics into multilayer piezo stacks remains a frontier that is still being explored [26]. Remarkably, to the author's knowledge, there are currently no commercially available transducers that combine the benefits of multilayer architecture with lead-free materials. In this context, the article aims to contribute to this current gap in research. To achieve this, the manufacturing process of BNT-BT samples is carried out, as well as the study of the possibility of improving its piezoelectric properties by Zr-doping. After the mechanical and electrical characterization, the EH performance of the manufactured piezo stacks is studied while varying the number of layers, level of Zr-doping, the electric load as well as the force excitation amplitude.

This article is structured as follows: Following an introductory Section 1, Section 2 provides a detailed account of the materials and methods, including the manufacturing process of the material, its mechanical and electrical characterization, and the experimental setup chosen to evaluate the energy harvesting performance of the multilayer samples. Section 3 presents the results and discussions of the aforementioned processes. Finally, Section 4 highlights the most remarkable conclusions drawn in this study.

2 Materials and methods

2.1 Preparation Process

The lead-free piezoceramics with a composition $0.95(Bi_{0.5}Na_{0.5})Ti_{1-x}O_3$-$0.05BaTi_{1-x}O_3$-$xZrO_2$ (BNT-5BT-xZr, x = 0, 0.5, 1, 2, 4 mol%) were obtained through the solid reaction method. Precursors, including Bi_2O_3 (Aldrich 99.9%), TiO_2 (Aldrich 99%), Na_2CO_3 (Biopack 99.5%), $BaCO_3$ (Biopack 99.5%), and ZrO_2 (Aldrich 99.9%), were weighed according to their stoichiometric proportion. Subsequently, they were milled in a planetary mill (Fritsch Pulverisette 7) with isopropyl alcohol (99%) as medium at 500 rpm for 12 cycles. Each cycle consisted of 30 minutes, the first 15 ones dedicated to active milling and the remaining 15 ones to rest. Later, the resulting powder was calcined at 850ºC for 2 hours, followed by a re-milled process under the same conditions as the aforementioned, although half the cycles. Finally, the resulting powder was mixed with PVA (Polyvinyl alcohol, J.T. Baker 99.0 - 99.8% fully hydrolyzed) as a binder and axially compressed at 40MPa, resulting in disk-shaped samples with 10 mm diameter and 1 mm of thinness. Last, these samples were sintered at 1150ºC for 2 hours (INDEF model 220).

2.2 Structural and microstructural characterization

The structural and microstructural characterization of the sintered samples was determined by density measurement, X-ray diffraction (XRD), and Field Emission Scanning Electron Microscopy (FE-SEM) techniques. Density was measured using the Archimedes method, considering the relationship between the mass of the specimen in air and the product between the difference in the mass of the specimen in air and water, and the density of the water, whereas the theoretical density was calculated by multiplying the number of atoms per unit cell by the atomic weight, and dividing by the result of the

product of the volume per unit cell multiplied by Avogadro's number. In this case, due to the low amount of ZrO_2 used in these samples, the same theoretical density (6.01 g/cm^3) was assumed for the calculation of the relative densities. The crystalline phases identification process was carried out by XRD analysis conducted with a PANalytical X'pert Pro equipment. XRD employed CuKα radiation (λ = 0.15406 nm) at a working voltage of 40 kV and a current of 100 mA, covering an angular range of 20-80 °2θ using a scanning speed of 0.02 º/s. For the deconvolution of the characteristic peaks, a 0.00125 º/s scanning speed was employed and the characteristics peaks were deconvolved using a pseudo-Voight function and a 0.6 shape factor. Finally, the microstructure was evaluated using a Hitachi S-4700 FE-SEM equipment. The surfaces of sintered samples were polished achieving a mirror finish, followed by a thermal treatment at 75 ºC below the sintering temperature for 25 minutes.

2.3 Electrical Characterization

The electrical characterization includes the measurement of the dielectric permittivity at room temperature, the piezoelectric constitutive constant $d_{33,}$ and the ferroelectric properties obtained by polarization vs. electric field (P-E) hysteresis loops. Before the electrical characterization, silver electrodes were painted on both plane-parallel faces. Dielectric permittivity at room temperature was measured using the Hewlett-Packard HP4284A impedance analyzer for a frequency of 1kHz. Regarding the measurement of the piezoelectric constant $d_{33,}$ the samples underwent poling through the application of a DC field of 4.0 KV/mm immersed in a silicone bath at a temperature of 90ºC. After poling, the piezoelectric constant was measured with the d_{33}-meter YE2730A (APC International, Ltd., USA). Finally, the P vs E measurements were conducted using a modified Sawyer-Tower circuit, with the sample immersed in a silicone bath at room temperature. The applied voltage was provided by a standard AC Hipot with a voltage range of 0 to 5000V. The measurement signal was acquired using an Owon SDS1022 oscilloscope with a resistive divider set at a ratio of 1:100.

2.4 Experimental procedure for energy harvesting

The experimental procedure for obtaining the harvested voltage of the lead-free multilayer actuators was conducted as follows: The piezoceramics disks were stacked varying the number of layers (1, 3, and 5) for the two BNT-5BT systems with different Zr compositions. In cases when more than one disk was used, electrical connections were made in parallel, and the poling direction orientation for two consecutive disks was chosen to be opposite to their neighbors. Moreover, copper sheets were inserted between the disks to act as electrodes, and connections were made by means of wires, collecting all positive and negative sheets into single terminals.

A representation of the experimental setup can be seen in **Fig. 1**, where it is possible to see a schematic view in **Fig. 1a** and a photo in **Fig. 1b**, as well as a detailed view of the piezo stack actuator in **Fig. 1c**. The system was mounted on an electrodynamic shaker capable of generating harmonic excitations with force amplitude between 0.1 and 10 Newtons and frequencies between 10 and 250 Hz. Force measurements were conducted using a Piezotronics 208C02 PCB load cell, while the voltage generated by the piezoelectric disks, in conjunction with force data, was recorded using an NI 9232 acquisition board at a rate of 4096 samples per second.

Several tests were carried out for the frequencies of 10, 50, 100, 150, 200, and 250 Hz, and for different electrical load resistances: R=326 kΩ, 130 kΩ, 56 kΩ. These tests were carried out for 1, 3, and 5 disks of the two systems of piezoceramics considered. Based on the variation of the current intensity on the electromechanical exciter, different force values were recorded for each case that varied between 1 and 10 Newtons. In turn, the capacity values for each of the cases were registered with a capacity meter.

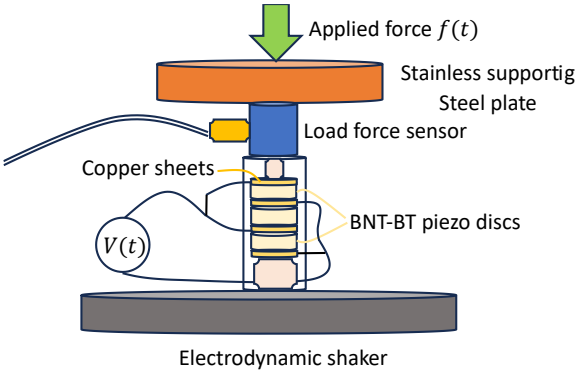

(a)

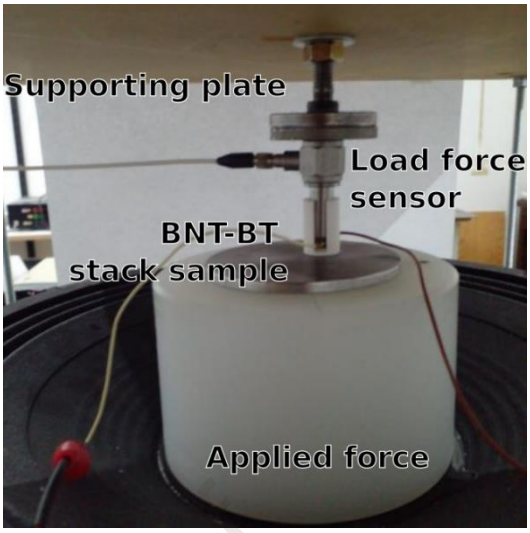

(b)

(c)

Fig. 1 (a) Schematic view, and (b) photo of the experimental set-up, (c) detailed view of the piezo stack.

3 Results and discussion

3.1 Materials Characterization

Piezoelectric generation constant ($g_{33}=d_{33}/\varepsilon_0\varepsilon'$) as a function of Zr concentration (BNT-5BT-xZr, x = 0, 0.5, 1, 2, 4 mol%) was analyzed to determine the most suitable Zr concentration for energy generation. **Fig. 2** shows the g_{33} values as a function of composition. It is observed that the piezoelectric voltage constant increases to a maximum for composition x = 2 mol% and subsequently decreases towards x = 4 mol% even falling below the undoped system. In addition, **Table 1** displays the

experimental and relative density values of the sintered samples. As it was observed in **Fig. 2**, the maximum density value was observed for composition x = 2 mol%, and the density value of the sample with 4 mol% also decreases below the undoped sample. Therefore, we will focus the characterization analysis on the composition x = 2 mol% (BNT-5BT-2Zr) and the obtained values will be compared with the undoped system (BNT-5BT, x=0), as a reference.

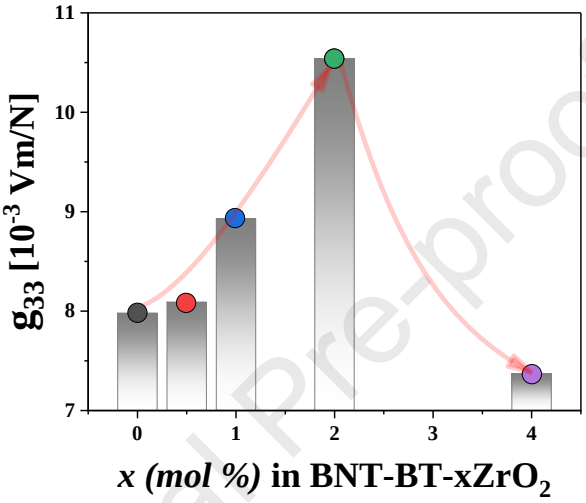

Fig. 2. Piezoelectric generation constant of BNT-5BT-xZr ceramics.

Table 1. Experimental (ρ) and relative density values of the sintered samples. Theoretical density=6.01 g/cm^3.

Sample	BNT-5BT	BNT-5BT-05Zr	BNT-5BT-1Zr	BNT-5BT-2Zr	BNT-5BT-4Zr
ρ (g/cm^3)	5.70	5.71	5.73	5.74	5.60
Relative density (%)	94.84	95.00	95.34	95.50	93.17

Fig. 3 shows the X-ray diffraction patterns at room temperature for samples with composition x = 0 and 2 mol%. In both compositions, the presence of a perovskite phase is confirmed, with the absence of secondary phases. Furthermore, in **Fig. 3b** it is evident that the proportion of the tetragonal phase increases concerning the rhombohedral phase with Zr addition. Moreover, a slight displacement of the peaks to lower angles with Zr addition can be observed. This peak shifting can be associated with the Zr^{4+} ion (ionic radius 0.72 Å, coordination VI) incorporation, at the B-site of the perovskite lattice,

instead of the Ti^{4+} ion with a lower ionic radius (0.605 Å, coordination VI) producing the expansion in the crystal lattice [27,28], while the gradual entry of Zr^{4+} ions into the BNT-5BT perovskite lattice produces an evolution in the crystal symmetry suppressing the rhombohedral phase in favor of the tetragonal phase.

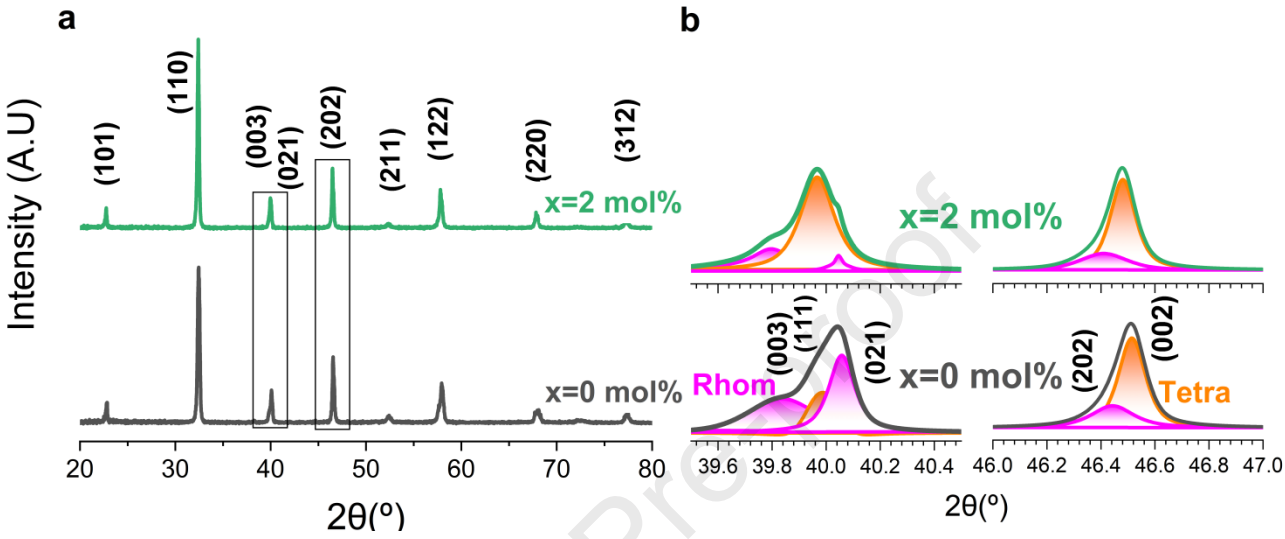

Fig. 3. XRD patterns of BNT-5BT-xZr (x = 0 and 2 mol%) sintered ceramics in the 2θ range **(a)** 20-80º y **(b)** 39.5-40.5/46.0-47.0º. Orange peaks are associated with the tetragonal phase, whereas the pink ones are related to the rhombohedral phase.

The grain size distribution was analyzed from the micrographs obtained by FE-SEM as illustrated in **Fig. 4.** As can be observed, both analyzed compositions present a dense microstructure with a reduced number of pores located at the grain edges, in addition, bimodal grain distributions with a mean size of 0.82 ± 0.42 μm for the undoped system and 1.36 ± 0.70 μm for the doped system are observed. The grain size increases for samples with x = 2.0 mol% compared to undoped samples. Ullah et al. also found that by increasing the doping of Zr the average grain size grew, and a denser microstructure with rounded and rectangular grains was determined [29]. However, Yao et al. determined a diminution in the grain sizes of BNT-BT-based ceramics for low Zr^{4+} addition, whereas an increment was observed for the higher amount of substitution [25]. The results presented by FE-

SEM and EDS (see **Fig. 5)** confirm that Zr^{4+} ions were partially included in the perovskite lattice. In fact, in addition to the incorporation in the perovskite lattice, ZrO_2 particles were segregated forming agglomerates. Consequently, considering that during the powder preparation, the complete incorporation of Zr^{4+} ions at the B-site ($0.95(Bi_{0.5}Na_{0.5})Ti_{1-x}O_3$-$0.05BaTi_{1-x}O_3$-$xZrO_2$) of the perovskite was assumed, doped samples resulted B-site deficient. In fact, during the calcination reaction of Ti-deficient BNT, B-site and oxygen vacancies with an amount proportional to the Ti-deficiency can be formed [30], according to Eq. (1).

$$0.25Na_2CO_3 + 0.25Bi_2O_3 + (1-x)TiO_2 \rightarrow Bi_{0.5}Na_{0.5}Ti_{1-x}V_{Ti(x)}^{''''}O_{3-2x}V_{O(2x)} + 0.25CO_2 \quad (1)$$

Finally, taking into account that in the samples, here reported, the majority component is $Bi_{0.5}Na_{0.5}TiO_3$, this Ti-deficit could be reduced by the evaporation of Bi_2O_3 (melting point 826 ºC) and Na_2O (melting point 851 ºC) during the sintering process (see Eq. 2).

$$Bi_{0.5}Na_{0.5}Ti_{1-x}V_{Ti(x)}^{''''}O_{3-2x}V_{O(2x)} \rightarrow (1-x)\,Bi_{0.5}Na_{0.5}TiO_3 + \frac{x}{4}(Na_2O + Bi_2O_3) \quad (2)$$

Certainly, these oxides could improve the sintering process via a transient molten phase before evaporation [30]. Furthermore, a free-zirconium secondary phase with a bar shape is observed. This phase is mostly composed of titanium, barium, and oxygen with a low amount of sodium (see **Fig. 5**).

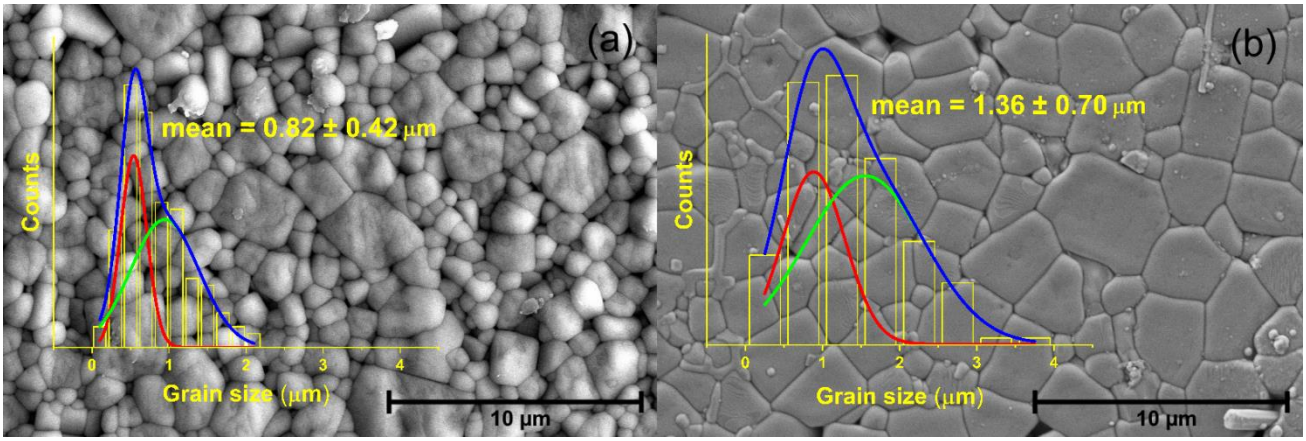

Fig. 4. FE-SEM micrographs and grain size distributions of BNT-5BT-xZr ceramics. **(a)** x = 0 mol%, **(b)** x = 2 mol%.

.

In order to analyze the ferroelectric behavior, the hysteresis curves of both samples were determined (**Fig. 6**). The comparison of these hysteresis cycles shows that the doped sample (Zr with x = 2 mol%) in the BNT-5BT system leads to an increase in the final polarizations of the sample, where the cycle is slightly slimmed by the decrease of the coercive field (E_c) from 41.72 kV/cm for the doped system to 39.35 kV/cm for the undoped case. In addition, P_r and P_{max} values increased from 24.98 and 30.08 μC/cm^2 to 29.97 and 36.70 μC/cm^2, for the undoped to the doped case respectively.

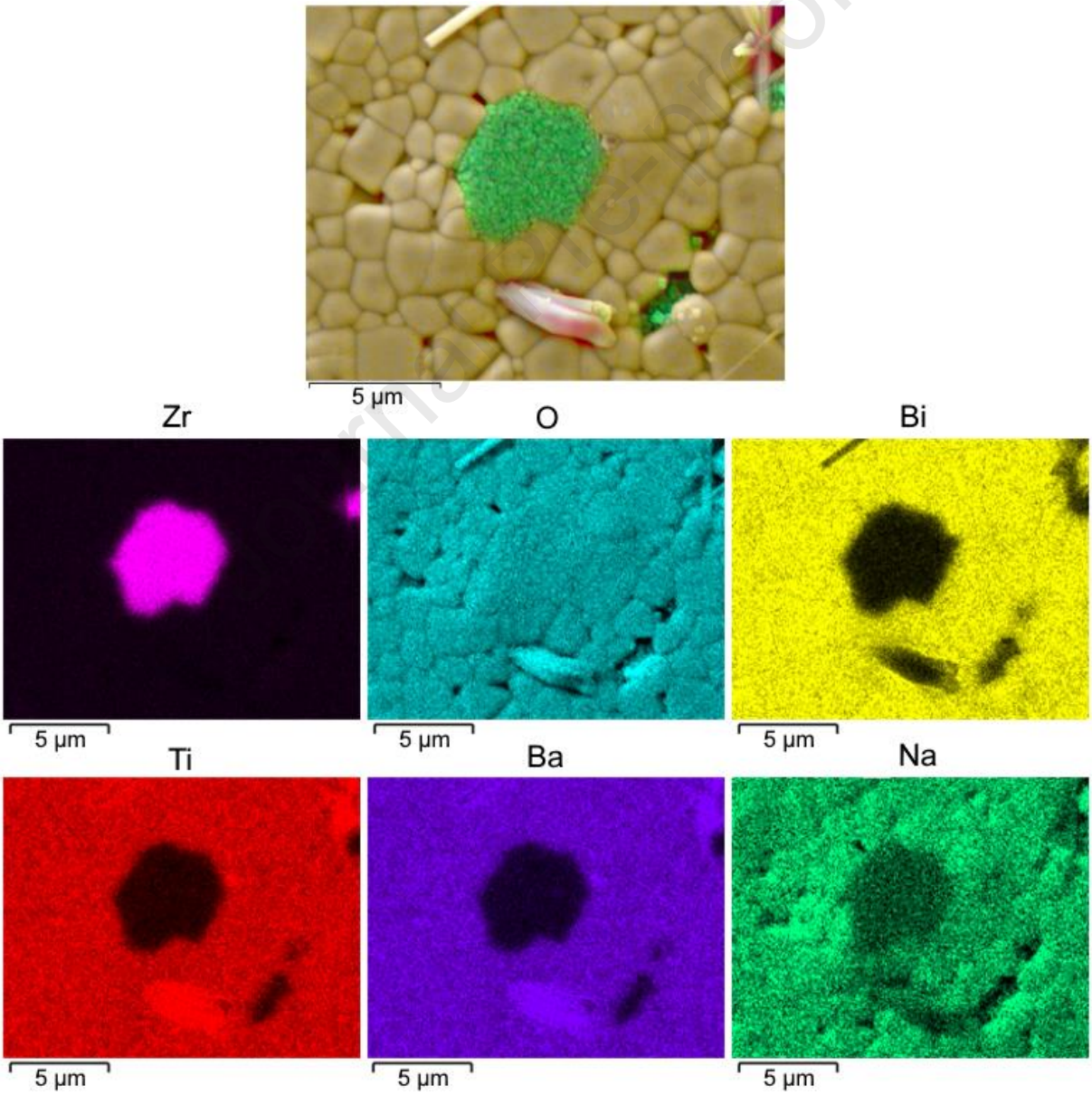

Fig. 5. Bidimensional elements distribution of BNT-5BT-2Zr sample.

Finally, piezoelectric constitutive constants (d_{33} and g_{33}), permittivity at room temperature (ε_{Troom}), and characteristic values of hysteresis loops: coercive field (E_c), remnant polarization (P_r) and maximum polarization (P_{max}) are summarized in **Table 2**, for the complete set of samples. In addition to the values of E_c, P_r, and P_{max} analyzed above, it can be observed that, as Zr-doping increases until 2 mol%, the piezoelectric constitutive parameters d_{33} and g_{33}, therefore, better energy harvesting properties are expected. This improvement in the piezoelectric values can be attributed to the changes observed in the average grain size and the stabilized phases. It is well known that piezoelectric properties are improved when grain growth and densification are increased [19,31]. For ferroelectric ceramics, larger grains facilitate domain motion increasing the ferroelectric and piezoelectric properties [32,33]. In addition, the stabilization of the morphotropic phase boundary improves the piezoelectric properties due to the existence of a higher degree of possible orientations for polarization under an electric field [19]. As a comparison, in **Table 2** piezoelectric and ferroelectric properties of BNT-xBT ceramics reported by other authors are included. Considering the influence of the $BaTiO_3$ amount in the BNT-xBT solid solution, it is known that Ba^{2+} substitution at the A-sites of BNT perovskite firstly assists the domain wall motion, and consequently, the relative permittivity increases [36]. However, when the content of Ba^{2+} reaches a certain critical value at the MPB, Ba^{2+} can replace Bi^{3+} creating oxygen vacancies that cause the domain walls clamping and consequently, the dielectric permittivity diminishes [34]. Taking into account, that the concentration where the MPB is reached is strongly dependent on the synthesis and processing conditions, variations in the dielectric, ferroelectric and piezoelectric properties are expected. Moreover, as the g_{33} coefficient increases when d_{33} rises and ε' diminishes, variations in this coefficient close to the MPB are registered. In particular, for the addition of zirconium, other researchers found a diminution in the remnant polarization, coercive field, and piezoelectric properties [25]. This behavior was attributed to the substitution of Zr^{4+} for Ti^{4+} which decreases the B-site deviation distance by moving atoms to body-centered locations, and destroying

the piezoelectric properties. In the samples here reported, the diminution in the piezoelectric properties was only registered for samples with x = 4 mol%

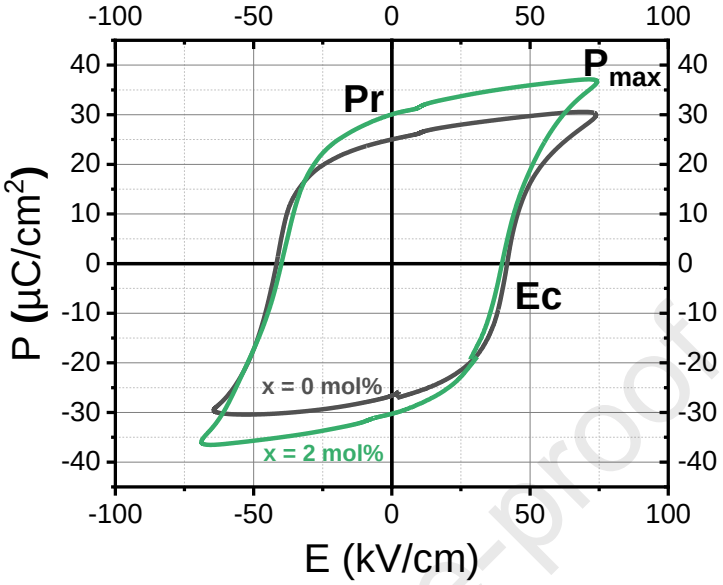

Fig. 6. Hysteresis loops of BNT-5BT-xZr (x = 0 and 2 mol%) sintered ceramics.

Table 2. Structural, piezoelectric and ferroelectric properties.

Sample	d_{33} (pC/N)	g_{33} (10^{-3}Vm/N)	ε'_{Troom}	E_c (kV/cm)	P_r (μC/cm^2)	P_{max} (μC/cm^2)	Ref.
BNT-5BT	110	8.0	1560	41.7	25.0	30.1	This work
BNT-5BT-05Zr	117	8.1	1636	40.2	28.2	31.8	This work
BNT-5BT-1Zr	127	8.9	1609	40.0	29.9	33.8	This work
BNT-5BT-2Zr	135	10.5	1508	39.3	30.0	36.7	This work
BNT-5BT-4Zr	90	7.4	1382	33.0	27.9	35.1	This work
BNT-6BT	178	25.4	770	30.0	28.2	32.3	[19]
BNT-7BT	134	3.2	4773	16.8	16.4	19.5	[34]
BNT-5BT	123	3.24	4300	24.3	7.2	11	[34]
BNT-6BT	189	10.7	2000	17.3	5.3	22.0	[35]
$(Bi_{0.5}Na_{0.5})_{0.94}Ba_{0.06}TiO_3$	141	7.6	2100	38.1	35.1	40	[25]

$(Bi_{0.5}Na_{0.5})_{0.94}Ba_{0.06}Zr_{0.01}Ti_{0.99}O_3$	125	-	.	27.0	31.1	38	[25]
$(Bi_{0.5}Na_{0.5})_{0.94}Ba_{0.06}Zr_{0.02}Ti_{0.98}O_3$	0	-	-	10.9	10.4	30	[25]

3.2 Piezoelectric Energy Harvesting (PEH)

In the experimental tests, the piezoelectric materials were subjected to an exciting force F to analyze the electrical charge when being mechanically stressed in d_{33} mode. The exciting force F was supposed to be a sinusoidal force of amplitude F_m, as $F = F_m \sin(\omega t)$ where ω is the angular exciting frequency. The stacked piezoelectric energy-harvesting units were prepared for both materials (BNT-5BT and BNT-5BT-2Zr) in different arrangements, including 1, 3, and 5 disks.

In the first test, the piezo stack was subjected to excitations at six different frequencies (10, 50, 100, 150, 200 and 250 Hz). This frequency range was chosen to considerate a spectrum where most of the mechanical vibrations to be harvested occurs. At each frequency, the stack was compressed by harmonic force with an amplitude of 10 N and considering open-circuit (OC) electrical condition. **Fig. 7a** and **7b** plot the measured amplitude of the output voltage versus loading frequencies, for BNT-5BT-2Zr and BNT-5BT materials, respectively. The results showed that the generated voltage was similar for both materials and due to the increasing rigidity of the stack, it increases for high-frequency values. For the maximum excitation frequency, the voltage generated with one disk was 0.457 V, for 3 disks was 1.188 V (an increase of 160%), and for the case of 5 disks, the increase was 275% (1.72 V).

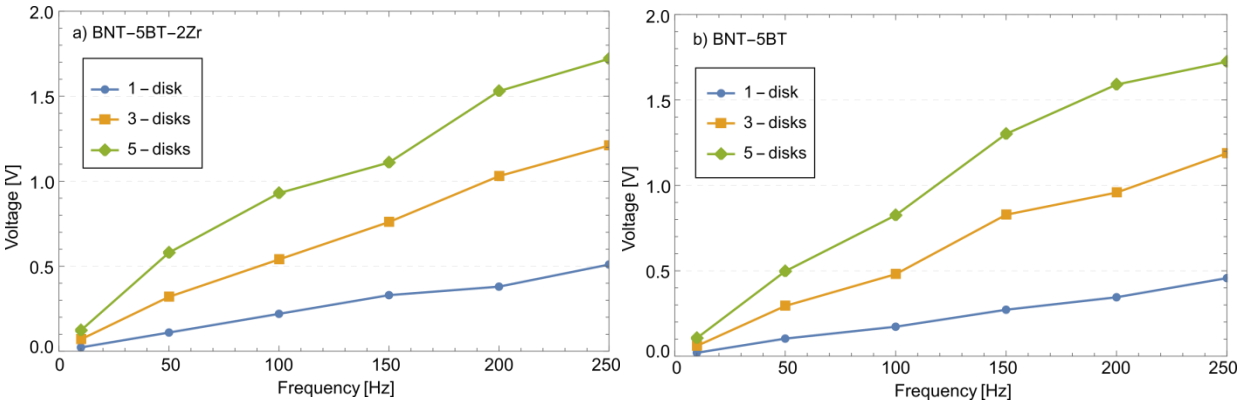

Fig. 7. Voltage output versus excitation frequency, a) BNT-5BT-2Zr and b) BNT-5BT, for a load of 10 N and OC conditions.

The performance output of these two materials for energy-harvesting was tested with varying load magnitude from 3 to 10 N. **Fig. 8** shows the output voltage versus load amplitude, for both materials (BNT-5BT-2Zr and BNT-5BT), considering open-circuit electrical conditions. As shown in **Fig. 8**, each curve corresponds to an excitation frequency ranging from 10 to 250 Hz. The highest values corresponded to the highest excitation frequency, while for the lowest excitation frequency (10 Hz), the values were of the order of 0.123 V with 5 disks and a maximum load of 10 N. The generated voltage increases as the load amplitude increases in a linear relationship. It can be seen from **Fig. 8** that the slope of these relationships was increased with frequency and the number of disks. However, in the case of the number of disks, it was observed that the increase in the slope was greater at low frequencies. For example, for 10 Hz the increase in slope was greater than three times between one disk and three disks and six times between one disk and five disks. In the case of 250 Hz the slope of the three-disk array was 2.37 greater than that of one disk and the slope of the five-disk array was 3.6 greater than that of one disk. These observations occurred in both materials with no significant changes.

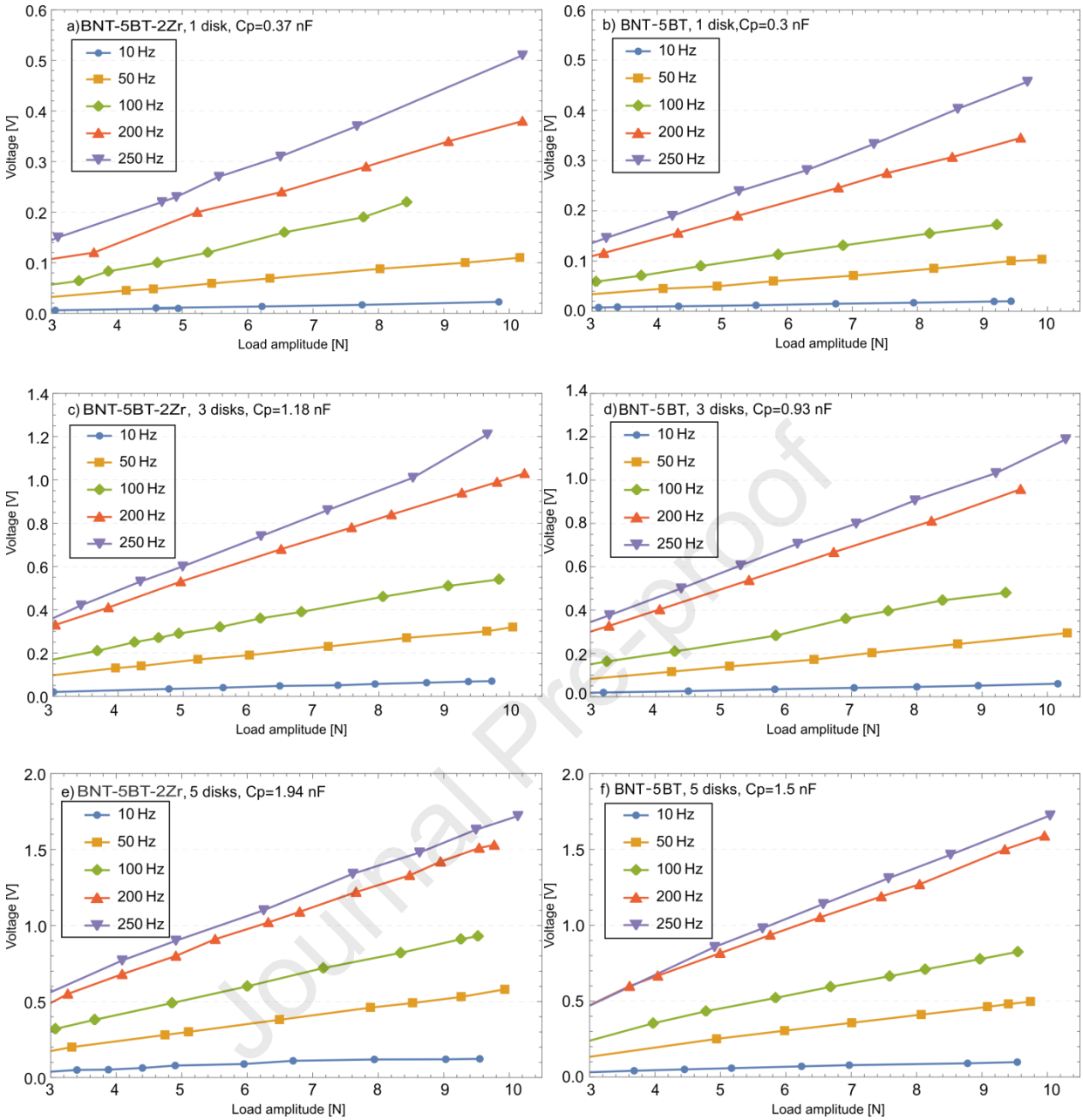

Fig. 8. Voltage output versus load amplitude, a, c and e) BNT-5BT-2Zr, and b, d and f) BNT-5BT, for various frequencies and OC conditions.

The influence of external resistance on the voltage versus various loading frequencies was examined for the array of five disks and a loading magnitude of 10 N. **Fig. 9** shows the generated voltage using external load resistance of 56, 130, and 323 kΩ. A similar tendency was observed for both materials (**Fig. 9a** and **9b**), however for the lowest values of resistive load the material without

additives (BNT-5BT) presents greater generation as the frequency increases, compared to the BNT-5BT-2Zr.

Comparing both materials, it is possible to observe in both **Fig. 8** and **Fig. 9** that no significant improvement in the voltage response was registered for the Zr-doped stack. This occurs because the total capacitance of the system was higherfor the stack formed by BNT-5BT-2Zr. For instance, for a 5-disk stack actuator, the capacitance of the one formed by BNT-5BT samples was 1.5 nF, while for the one formed by BNT-5BT-2Zr, it was 1.94 nF.

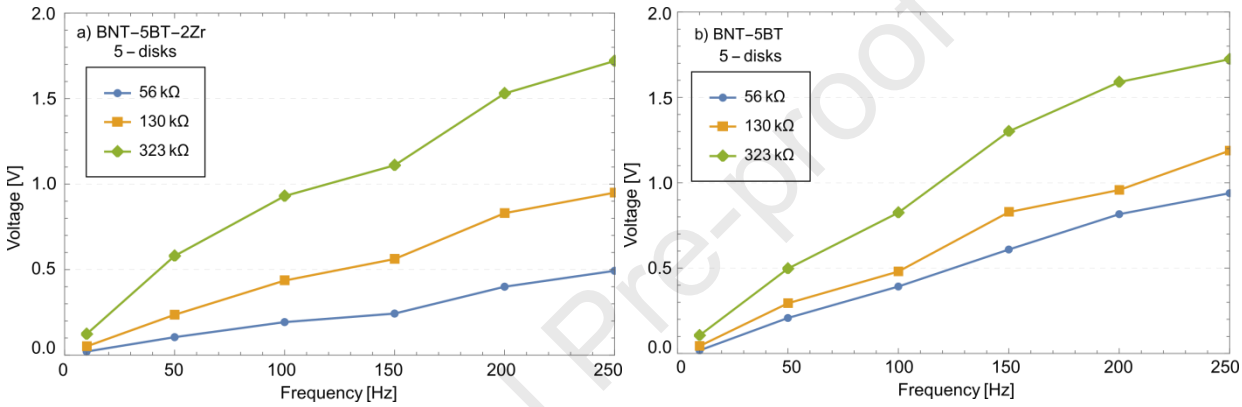

Fig. 9. Voltage output versus loading frequency for R= 56, 130, and 323 kΩ, a) BNT-5BT-2Zr and b) BNT-5BT, for a loading magnitude 10 N.

3.3 Effective d_{33} identification

The governing circuit equation of a stack is governed by the following expression, considering that the stack consists of *N* disks connected in parallel to a resistive electrical load (*R*).

$$\sum_{i=1}^{N} \frac{d}{dt}\left(\int_{A_i} \mathbf{D}\cdot\mathbf{n}dA_i\right) = \frac{v(t)}{R} \tag{3}$$

where *v(t)* is the voltage generated by the piezoelectric stack, **D** is the electric displacement vector, **n** is the vector of surface normal of the electrodes with area A_i of the *i*-th disk. The electric displacement is related to the electric field E_j and the stress tensor T_{jk} by the piezoelectric constitutive equation

$$D_i = d_{ijk} T_{jk} + \varepsilon_{ij}^T E_j \tag{4}$$

where d_{ijk} represents the tensor of piezoelectric strain constants and ε_{ij}^T is the tensor of permittivity constants at constant stress. The natural frequency of the stack in the axial direction is very far from the excitation frequency. So, in this model, the mechanical equation is not considered to analyze electromechanical system dynamics [37]. Then, the governing electromechanical equation is obtained for the piezoelectric stack subjected to a uniaxial dynamic excitation considering the stress on the thickness (h) of each piezo-electric disk $T= p(t)$ and the electric field $E=-v/h$.

$$C_p^{eq} \dot{v}(t) + \frac{v(t)}{R} = d_{33}^{eff} \dot{F}(t) \tag{5}$$

Where $F(t) = Ap(t)$ is the dynamic load, the dot implies differentiation with respect to time, A is the cross-sectional to the stack, C_p^{eq} and d_{33}^{eff} are the equivalent capacitance and the effective piezoelectric constant, respectively. In order to attain the electromechanical frequency response of the stack, the dynamic load was harmonic with $p(t) = p_0 e^{j\omega t}$ (where p_0 is the loading amplitude) being ω the loading frequency. The steady-state voltage response is assumed to be $v(t) = Ve^{j\omega t}$ and then solving Eq. (5) the complex voltage V can be expressed as:

$$V = \frac{j\omega A d_{33}^{eff} p_0}{j\omega C_p^{eq} + 1/R} \tag{6}$$

Finally, the power output of the stack is calculated via

$$P = \frac{|V|^2}{R} = \frac{\left(\omega A d_{33}^{eff} p_0\right)^2 R}{\left(\omega C_p^{eq} R\right)^2 + 1} \tag{7}$$

Similar power values were obtained for both materials, so in this case, the analysis is concentrated on the material with additive BNT-5BT-2Zr. **Fig. 10** shows the generated power versus load resistance for a sample of five disks made of BNT-5BT-2Zr, considering two values of loading magnitude 2.5

and 5 N (dotted lines). Using the maximum power-transfer theorem that occurs when the external electrical impedance matches the internal impedance of the stack, the following expression is obtained:

$$P_{\max} = P\big|_{R=R^*} = \frac{\omega\left(Ad_{33}^{eff}\, p_0\right)^2}{2C_p^{eq}} \tag{8}$$

where R^* is the optimal electrical load. From the last expression, it is possible to calculate the effective electromechanical coefficient d_{33}^{eff} using the maximum power value recorded experimentally (see **Fig. 10**). In this way, using Eq. (8), the values obtained are d_{33}^{eff} = 588 and 625 pC/N, for a loading magnitude of 2.5 and 5 N, respectively. These values are in agreement with those of **Table 2** if we apply an expression like the one presented by Xu *et al.* [13].

$$d_{33}^{eff} = cnd_{33} \tag{9}$$

Where c is a constant between 0 and 1 and n is the number of the piezo layers. By using Eq. (9) and assuming $c = 0.95$ (a typical value) we obtain an average value of $d_{33} = 128$ pC/N which differs by less than 5% from the value of **Table 2** ($d_{33} = 135$ pC/N).

The experimental measurements of harvested power were compared to analytical solutions computed using Eq. (7). For harmonic excitation at 250 Hz, the comparisons are shown in **Fig. 10** as the power output per stack volume, i.e. power density of the harvester. Then substituting these values into the power expression (Eq. 7), power versus electrical resistance is graphed in **Fig. 10** (solid lines), where a good fit between the experimental and the analytical results was observed.

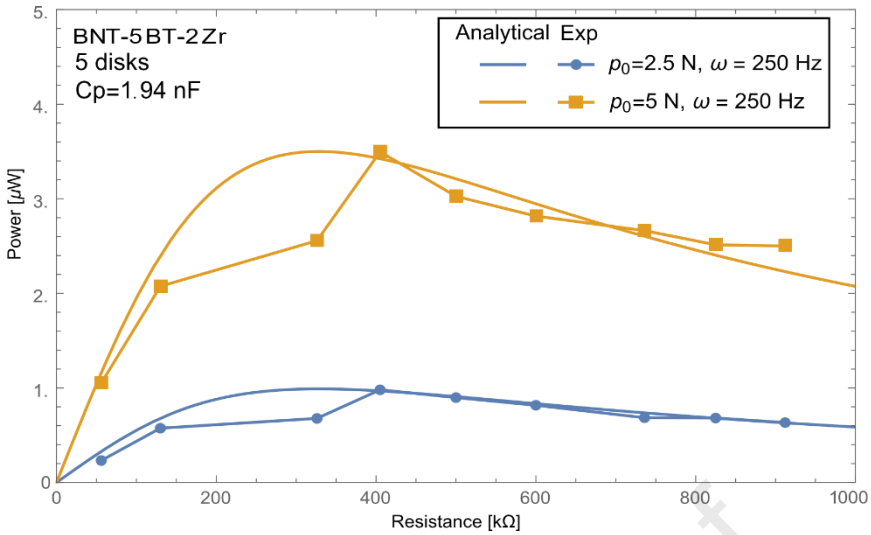

Fig. 10. Power output versus electrical load resistance under harmonic excitation at 250 Hz for 5 disks of BNT-5BT-2Zr, considering two loading magnitudes 2.5 and 5 N.

4 Conclusions

In this study, the potential use of lead-free multilayer piezo stacks as a source of voltage generation for energy harvesting is explored. The research aims to analyze the influence of zirconium (Zr) doping on a lead-free piezoelectric BNT-BT (BNT-5BT) sample within multilayer piezo stacks. Four different concentrations of Zr-doped samples (BNT-5BT-xZr, x = 0, 0.5, 1, 2, 4 mol%) were manufactured and subjected to structural, microstructural, and electrical characterization. Unexpectedly, an increase in grain size was observed in samples with x = 2.0 mol%, contrary to anticipated results based on existing research. Scanning Electron Microscopy (SEM) and Energy Dispersive Spectroscopy (EDS) analyses confirmed that Zr^{4+} ions were partially integrated into the perovskite lattice and the excess of ZrO_2 was segregated, forming agglomerates. Additionally, the ZrO_2 addition caused an increase in both the average grain size and the tetragonal to rhombohedral phases proportion.

Piezoelectric constitutive constants d_{33} and g_{33}, density ρ, permittivity at room temperature ε_{Troom}, and characteristic values of hysteresis loops coercive field E_c, remnant polarization P_r, and maximum polarization P_s were determined through measurements. The findings indicate that Zr doping enhances the piezoelectric constitutive parameters d_{33} and g_{33}. Notably, samples with x = 2.0

mol% exhibit the highest piezoelectric parameters. Various electromechanical tests were conducted using piezo samples configured into multilayer stacks comprising 1, 3, and 5 disks, both for BNT-5BT with and without Zr (doped with x = 2.0 mol%). These tests revealed that, when subjected to varying sinusoidal force magnitude, frequency, and electric load, the multilayer piezo stacks could generate up to 1.5 Volts (peak) under conditions of 250 Hz, 10 N load, and an open circuit (OC) setup, in the scenario where the stack consists of 5 disks. Furthermore, the tests demonstrated an increase in generation with higher load, frequency, electric load, and number of disks. Employing a simple mathematical model, an effective d_{33}^{eff} piezo constant was computed. This value allows us the generation of distinct power curves as a function of electric load for two different mechanical loads. Theoretical curves were found to align with experimental results, confirming their agreement. Comparison between the effective piezo constant d_{33}^{eff} calculated via the model and that obtained using a standard d_{33} meter showed reasonable agreement.

Funding

The authors would like to thank Universidad Nacional de Mar del Plata (Argentina), Universidad Tecnológica Nacional (Argentina), Universidad Nacional del Sur (Argentina), Agencia Nacional de Promoción Científica y Tecnológica (ANPCyT) and Consejo Nacional de Investigaciones Científicas y Técnicas (CONICET).

References

[1] Liu, H., Zhong, J., Lee, C., Lee, S. W., & Lin, L. (2018). A comprehensive review on piezoelectric energy harvesting technology: Materials, mechanisms, and applications. *Applied Physics Reviews*, 5 043106

[2] Erturk, A., Tarazaga, P. A., Farmer, J. R., & Inman, D. J. (2009). Effect of strain nodes and electrode configuration on piezoelectric energy harvesting from cantilevered beams. *Journal of Vibration and Acoustics*, 131 (1) 011010.

[3] Moure, A., Rodríguez, M. I., Rueda, S. H., Gonzalo, A., Rubio-Marcos, F., Cuadros, D. U., ... & Fernández, J. F. (2016). Feasible integration in asphalt of piezoelectric cymbals for vibration energy harvesting. *Energy Conversion and Management*, 112, 246-253.

[4] Jasim, A., Wang, H., Yesner, G., Safari, A., & Maher, A. (2017). Optimized design of layered bridge transducer for piezoelectric energy harvesting from roadway. *Energy*, 141, 1133-1145.

[5] Smart Materials: https://www.smart-material.com/

[6] MIDE Technology: https://www.mide.com/

[7] APM Ceramics: https://www.americanpiezo.com/

[8] Wang, C., Wang, S., Gao, Z., & Wang, X. (2019). Applicability evaluation of embedded piezoelectric energy harvester applied in pavement structures. *Applied Energy*, 251, 113383.

[9] PiezoDrive: https://www.piezodrive.com

[10] PiezoTechnics: https://www.piezotechnics.com/

[11] Wang, C., Song, Z., Gao, Z., Yu, G., & Wang, S. (2019). Preparation and performance research of stacked piezoelectric energy-harvesting units for pavements. *Energy and Buildings*, 183, 581-591.

[12] Khalili, M., Biten, A. B., Vishwakarma, G., Ahmed, S., & Papagiannakis, A. T. (2019). Electro-mechanical characterization of a piezoelectric energy harvester. *Applied Energy*, 253, 113585.

[13] Xu, T. B., Siochi, E. J., Kang, J. H., Zuo, L., Zhou, W., Tang, X., & Jiang, X. (2013). Energy harvesting using a PZT ceramic multilayer stack. *Smart Materials and Structures*, 22(6), 065015.

[14] Panda, P. K. (2009). Environmental friendly lead-free piezoelectric materials. *Journal of Materials Science*, 44, 5049-5062.

[15] Maqbool, A., Hussain, A., Rahman, J.U., Kwon Song, T., Kim, W.J., Lee, J., & Kim, M.H. (2014). Enhanced electric field-induced strain and ferroelectric behavior of $(Bi_{0.5}Na_{0.5})TiO_3$–$BaTiO_3$–$SrZrO_3$ lead-free ceramics, *Ceramics International*, 40 (8, PartA), 11905-11914.

[16] Kumari, K., Prasad, A., & Prasad, K. (2010). Structural and Dielectric Properties of $(Bi_{1/2}Na_{1/2})TiO_3$-WO_3 Ceramics, *Materials Science*, 16 (4), 287-291.

[17] Hussain, A., Jabeen, N., Hassan, N.U., Rasheed, S., Idrees, A., Eldin, S.M., Ouladsmane, M., Khan, S., Akkinepally, B., & Javed, M.S. (2023). Structural, piezoelectric and ferroelectric analysis of $0.96Bi_{0.5}Na_{0.5}TiO_3$-$0.06BaTiO_3$:xwt%$MnO_2$ ceramics for high-tech applications, *Ceramics International*, 49 (17, PartA), 27848-27854.

[18] Difeo, M., Osinaga, S., Febbo, M., Machado, S. P., Castro, M., & Ramajo, L. (2021). Influence of the $(Bi_{0.5}Na_{0.5})TiO_3$–$BaTiO_3$ lead-free piezoceramic geometries on the power generation of energy harvesting devices. *Ceramics International*, 47(8), 10696-10704.

[19] Jaita. P., Manotham. S., & Rujijanagul, G. (2020). Influence of Al_2O_3 nanoparticle doping on depolarization temperature, and electrical and energy harvesting properties of lead-free $0.94(Bi_{0.5}Na_{0.5})TiO_3$–$0.06BaTiO_3$ ceramics. *RSC Advances.* 53 (10), 32078-32087.

[20] Ozgul. M., & Kucuk. A. (2016). B_2O_3 doping in $0.94(Bi_{0.5}Na_{0.5})TiO_3$-$0.06BaTiO_3$ lead-free piezoelectric. *Ceramics International.* 42 (16), 19119-19123.

[21] Lin, D., Xiao, D., Zhu, J., Yu, P. (2006). Piezoelectric and ferroelectric properties of lead-free $[Bi_{1-y}(Na_{1-x-y}Li_x)]_{0.5}Ba_yTiO_3$ ceramics. *Journal of the European Ceramic Society*, 26 (15), 3247-3251.

[22] Difeo, M., Ramajo L., & M. Castro, M. (2021). Influence of CuO addition on dielectric and piezoelectric properties of $(Bi_{0.5}Na_{0.5})TiO_3$–$BaTiO_3$ lead-free piezoceramics, *Journal of Advanced Dielectrics*, 11 (3), 214004.

[23] Armstrong, R., Morgens, E. Maurice, K., & Buchanan, C. (1989). Effects of Zirconia on Microstructure and Dielectric Properties of Barium Titanate Ceramics. *Journal of the European Ceramic Society* 72 (4), 605-11.

[24] Rachakom, A., Jiansirisomboon, S., & Watcharapasorn, A. (2014). Effect of poling on piezoelectric and ferroelectric properties of $Bi_{0.5}Na_{0.5}Ti_{1-x}Zr_xO_3$ ceramics. *Journal of Electroceramics*, 33(1-2), 105–110.[25] Yao, Y.-Q., Tseng, T.-Y., Chou, C.-C., & Chen, H. H. D. (2007). Phase transition and

piezoelectric property of $(Bi_{0.5}Na_{0.5})0.94Ba_{0.06}ZryTi_{1-y}O_3$(y=0–0.04) ceramics. *Journal of Applied Physics*, 102(9), 094102.

[26] Spitsin, A. I., Khramtsov, A. M., Segalla, A. G., Bush, A. A., & Kamentsev, K. E. (2019). Research and development of high temperature multilayer piezo stack based on $Na_{0.5}Bi_{4.5}Ti_4O_{15}$ lead-free ceramic system produced by tape-casting slurry technology. *Ferroelectrics*, 539(1), 134-140.

[27] Hussain, A., Ahn, C. W., Lee, J. S., Ullah, A., & Kim, I. W. (2010). Large electric-field-induced strain in Zr-modified lead-free $Bi_{0.5}(Na_{0.78}K_{0.22})_{0.5}TiO_3$ piezoelectric ceramics. Sensors and Actuators A: Physical, 158(1), 84–89.

[28] Database of Ionic Radii: http://abulafia.mt.ic.ac.uk/shannon/

[29] Ullah, A., Ullah, M., Ullah, A., Ullah, A., Saddiq, G., Ullah, B., … Kim, I. W. (2019). Dielectric and Electromechanical Properties of Zr-Doped BNT-ST Lead-Free Piezoelectric Ceramics. *Journal of the Korean Physical Society*, 74(6), 589–594.

[30] Naderer, M., Kainz, T., Schütz, D., & Reichmann, K. (2014). The influence of Ti-nonstoichiometry in $Bi_{0.5}Na_{0.5}TiO_3$. Journal of the European Ceramic Society, 34(3), 663–667.

[31] Sezer, N., & Koç, M. (2021). A comprehensive review on the state-of-the-art of piezoelectric energy harvesting. *Nano Energy*, 80, 105567.

[32] Mudinepalli, V.R., Feng, L., Lin, W. C. & Murty, B. S. (2015). Effect of grain size on dielectric and ferroelectric properties of nanostructured $Ba_{0.8}Sr_{0.2}TiO_3$ ceramics. *Journal of Advanced Ceramics*, 4, 46 —53.

[33] Randall**,** C.A., Kim**,** N., Kucera**,** J.P., Cao**,** W. **&** Shrout, T.R. (1998). Intrinsic and Extrinsic Size Effects in Fine-Grained Morphotropic-Phase-Boundary Lead Zirconate Titanate Ceramics. *Journal of the American Ceramic Society*, 81 **(3)**, 677 —688

[34] Parija, B., Badapanda, T., Panigrahi, S., & Sinha, T. P. (2013). Ferroelectric and piezoelectric properties of $(1-x)(Bi_{0.5}Na_{0.5})TiO_3$–$xBaTiO_3$ ceramics. *Journal of Materials Science: Materials in Electronics*, 24, 402–410 10.1007/s10854-012-0764-z

[35] Manotham, S., Jaita, P., Butnoi, P., Lertcumfu, N., & Rujijanagul, G. (2022). Improvements of depolarization temperature, piezoelectric and energy harvesting properties of BNT-based ceramics by doping an interstitial dopant. *Journal of Alloys and Compounds*, 897, 163021.

[36] Kang, W.S., & Koh, J.H. (2015). $(1-x)Bi_{0.5}Na_{0.5}TiO_3$–$xBaTiO_3$ lead-free piezoelectric ceramics for energy-harvesting applications. *Journal of the European Ceramic Society*, 35 (7), 2057–2064.

[37] Erturk, A., & Inman, D. J. (2011). Piezoelectric energy harvesting. *John Wiley & Sons*.

Declaration of interests

☒ The authors declare that they have no known competing financial interests or personal relationships that could have appeared to influence the work reported in this paper.

☐ The authors declare the following financial interests/personal relationships which may be considered as potential competing interests: